Applied Physics Letters

Ultra-low threshold green InGaN quantum dot microdisk lasers grown on silicon

Cite as: Appl. Phys. Lett. **117**, 031104 (2020); https://doi.org/10.1063/5.0012045
Submitted: 27 April 2020 . Accepted: 13 July 2020 . Published Online: 22 July 2020

Chunyu Zhao, Chak Wah Tang, Jiannong Wang, and Kei May Lau

Ultra-low threshold green InGaN quantum dot microdisk lasers grown on silicon

Cite as: Appl. Phys. Lett. **117**, 031104 (2020); doi: 10.1063/5.0012045
Submitted: 27 April 2020 · Accepted: 13 July 2020 ·
Published Online: 22 July 2020

Chunyu Zhao,[1,2] Chak Wah Tang,[1] Jiannong Wang,[2] and Kei May Lau[1,a)]

AFFILIATIONS

[1]Department of Electronic and Computer Engineering, Hong Kong University of Science and Technology, Clear Water Bay, Kowloon, Hong Kong
[2]Department of Physics, Hong Kong University of Science and Technology, Clear Water Bay, Kowloon, Hong Kong

[a)]Author to whom correspondence should be addressed: eekmlau@ust.hk. **Tel.:** (852)23587049. **Fax:** (852) 23581485.

ABSTRACT

We report ultra-low threshold green InGaN quantum-dot (QD) microdisk lasers directly grown on Si substrates by metal-organic chemical vapor deposition. Vertically stacked InGaN/GaN QDs by epitaxy on Si were adopted as the microcavity gain medium. Under continuous-wave optical pumping, we observed room temperature lasing at 522 nm from the microcavity lasers with a diameter of 1.0 μm and obtained an ultra-low threshold of 76 W/cm^2. The sidewall roughness values of the microdisk lasers etched by different solutions of potassium hydroxide and HF/HNO_3 were compared. We detected a strong correlation between the lasing thresholds and the sidewall roughness of the microdisk lasers, with the lasing threshold improved from 1.6 kW/cm^2 to below 100 W/cm^2 and the full width at half maximum reduced from 0.53 nm to 0.2 nm through smoothing of the sidewall.

III-nitride semiconductors have attracted increasing attention for electronic and optoelectronic applications due to their direct energy bandgap and wide wavelength emission.[1,2] The demonstrations of high-performance high electron mobility transistors (HEMTs),[3] photodetectors (PDs),[4] light emitting diodes (LEDs),[5] and laser diodes (LDs)[6] manifest the diverse applications of this material system. In particular, III-nitride green light emitters are being developed due to their potential application in full color displays, optical data storage, mobile projectors, visible light communications, and military applications.[7–10] GaN microdisk lasers feature a simple fabrication process and an ultra-small footprint.[11] In addition, microdisk lasers with low-loss whispering gallery (WG) modes possess some distinct advantages such as low thresholds and high quality factors (Q-factors).[12–14] In contrast to undercutting GaN microdisk lasers on sapphire substrates using photoelectrochemical (PEC) etching, microdisk lasers directly grown on Si are easily fabricated through selectively etching of Si.[15] Additionally, integrating GaN microdisk lasers on Si might open an alternative path toward large-scale, multi-functional, and low-cost Si-based photonic integrated circuits (PICs).[16,17]

The first optically pumped GaN microdisk laser on Si was fabricated by a combination of dry and wet etching, with a lasing wavelength of 365 nm at low temperature (4.3 K).[15] After that, optically pumped III-nitride quantum well (QW) microdisk lasers on Si from green to deep ultra-violet were demonstrated.[18–20] Until now, GaN-based microdisk lasers grown on Si still have many challenges for electrically pumped lasing due to the epitaxial material quality and device fabrication.[21] The room-temperature thresholds of optically pumped QW microdisk lasers are generally reported in the range of a few hundred kW/cm^2 [for continuous-wave (CW) measurements] or a few mJ/cm^2 (for pulsed measurements).[22] Low-threshold microdisk lasers with QWs as active gain media remain a challenge. Possible reasons include poor crystal quality of InGaN materials with a high indium content and/or severe non-radiative recombination via surface states in the periphery. Three-dimensional confinement of carriers in quantum dots (QDs) allows for lower sensitivity to structural defects and thus makes them better candidates as the active layer of microcavity lasers. In addition, QD lasers have also been demonstrated to exhibit a high Q-factor and ultra-low threshold.[23,24] GaN-based QDs can be achieved by the Stranski–Krastanov (SK) growth mode or modified droplet epitaxy (MDE) method.[23,25] GaN QD microdisk lasing at a wavelength of ∼310 nm has been demonstrated with a low threshold power density of 20 kW/cm^2 and a Q-factor of 5000.[26] A low lasing threshold of 0.28 mJ/cm^2 has been achieved in InGaN QD microdisk lasers in the blue spectral range.[27] Recently, a record-low lasing threshold of 6.2 μJ/cm^2 has been achieved in GaN microdisks with InGaN QDs, emitting at ∼440 nm.[25] However, there has been no demonstration of green-emitting QD microdisk lasers. In this work, we report extremely low-threshold lasing in green QD microdisk lasers directly grown on Si (111) substrates. A structure comprising three layers of vertically aligned InGaN/GaN QDs was selected as the gain medium. The fabricated lasers exhibit room temperature lasing with a threshold excitation density of 76 W/cm^2 under CW optical excitation. We also discuss the influences of microcavity sidewall roughness on the laser performance.

We performed the GaN growth on 2-in. Si (111) substrates using an Aixtron close-coupled showerhead (CCS) metal-organic chemical vapor deposition (MOCVD) system with an *in situ* monitoring system (LayTec EpiTT). Trimethylgallium (TMGa), trimethylaluminum (TMAl), and ammonia (NH_3) were used as the Ga, Al, and N sources during the AlN and GaN buffer layer growth. Hydrogen (H_2) was used as the carrier gas. For the InGaN QD and GaN barrier layer growth, triethylgallium (TEGa), trimethylindium (TMIn), and NH_3 were employed as precursors and nitrogen (N_2) as a carrier gas. Figure 1(a) schematically depicts the epitaxial structure of the microdisk lasers on Si. Before growth, oxide desorption of the Si substrates was performed at 1000 °C for 10 min. Then, a 180-nm-thick AlN seed layer was deposited to prevent melt-back etching caused by the Ga–Si alloys. This AlN buffer layer improves the crystalline quality of the subsequent GaN buffer and builds up the compressive strain to compensate for the tensile strain during the cooldown period. Next, a 240-nm thick n-type GaN buffer layer was grown at 1050 °C on the AlN layer to obtain a smooth surface for the subsequent QD growth. A three-pair InGaN (2.5 nm)/GaN (10 nm) QD structure was grown as the active region. The growth pressure was kept at 400 mbar, and a V/III ratio of 1×10^4 was used. The InGaN QDs and GaN barrier were grown at 670 °C and 830 °C, respectively. A 90-nm GaN cap layer was subsequently grown at 890 °C.

Figure 1(b) presents a cross-sectional transmission electron microscopy (TEM) image of the as-grown sample with the three-stacked InGaN/GaN QD structure. It can be clearly seen that a substantial proportion of the threading dislocations (TDs) were filtered out by the AlN and GaN buffer layers. Figure 1(c) displays a zoomed-in TEM image of the three-stacked QD active region, revealing uniform and vertically aligned QDs. The thickness of each layer agrees well with the designed parameters. The InGaN QDs separated by GaN barrier layers are clearly shown to exhibit self-organized growth along the vertical direction. The InGaN QDs in the first layer produce a tensile strain in the GaN layer above the QDs. The distribution of the strain field in the first GaN barrier layer provides an energetically favorable region for the successive growth of InGaN QDs. Therefore, the vertically aligned InGaN QDs can be clearly observed due to the strain contrast of the QDs in the two layers.[28] It should be pointed out that this vertically aligned and well-separated QD structure is strong evidence of self-assembled QDs grown by the SK growth mode.[29] The good crystalline quality of the active region is attributed to the effective defect trapping and reduction scheme offered by the AlN buffer. The QDs grown on Si present good uniformity with a density of $\sim 1 \times 10^{10}$ cm^{-2} and a height of ~2.5 nm. The diameter and spacer of the QDs range from 33 to 64 nm and 50–60 nm, respectively. The disk-like shape with a large width to height ratio is a typical signature of self-assembled InGaN QDs grown in SK growth mode.[30–32]

We characterized the QDs using room temperature photoluminescence (PL) measurements. A CW diode laser emitting at 405 nm was used through a high (0.95) numerical aperture (NA) objective lens normal to the surface of the sample. The excitation light was focused to a spot size of approximately 2.0 μm in diameter. The luminescence from the sample was collected through the same objective. Figure 1(d) shows the normalized PL spectra at room temperature from the as-grown InGaN QD microdisk lasers on Si substrates at increasing excitation power density from 0.4 kW/cm^2 to 47.8 kW/cm^2. The peak wavelength from these as-grown QDs on the Si sample is located at 545 nm with a full width at half maximum (FWHM) of 43 nm at an excitation power density of 0.4 kW/cm^2. With a 100-fold increase in excitation power to 47.8 kW/cm^2, the peak PL wavelength shifts to 529 nm with the same FWHM of 43 nm. This blueshift is typical for InGaN/GaN heterostructures with large polarization fields.[33] The unchanged FWHM suggests the excellent uniformity of the InGaN QDs.

Microdisk lasers with a diameter of ~1.0 μm were fabricated using silica microsphere lithography, followed by inductively coupled plasma (ICP) etching and selectively wet etching, as schematically summarized in Fig. 2. Initially, the epi-wafer with a grown QD laser

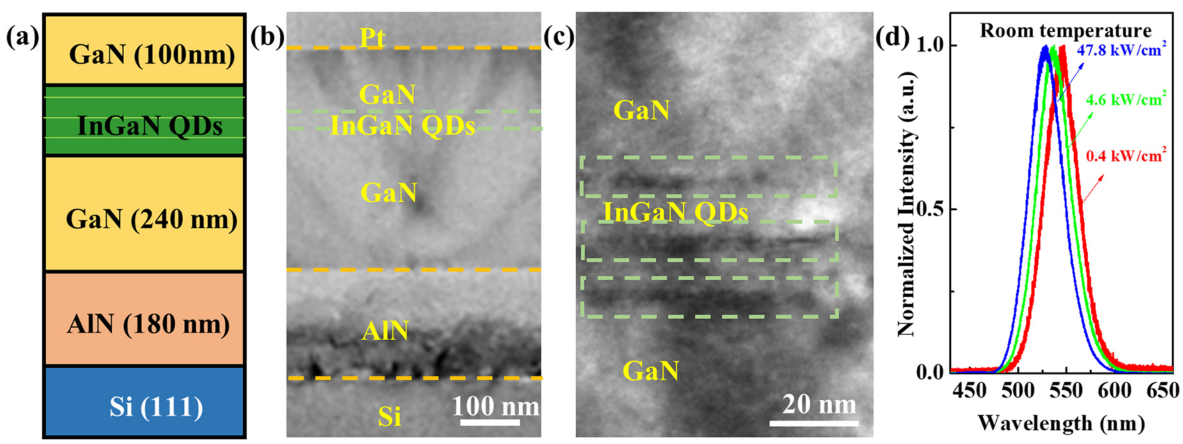

FIG. 1. (a) Schematic illustration of the epitaxial structure of material in the disk region; cross-sectional TEM image of (b) the microdisk structure and (c) the three-stacked InGaN QDs; (d) room temperature PL spectra of the as-grown QD microdisk lasers on Si substrates at increasing excitation power densities from 0.4 kW/cm^2 to 47.8 kW/cm^2.

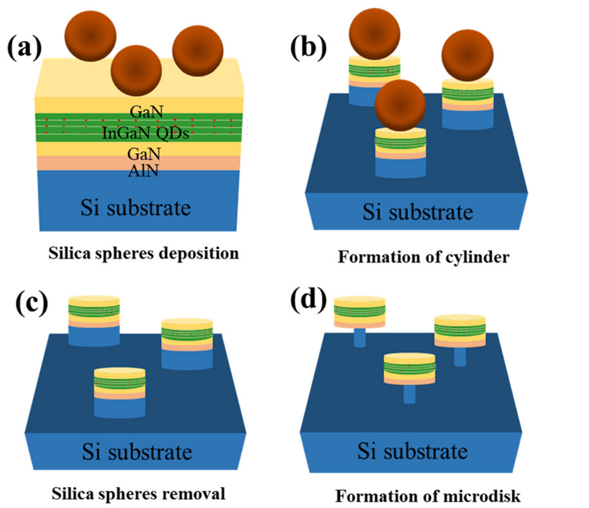

FIG. 2. Schematic process flow of the microdisk lasers. (a) 1.0 μm silica sphere deposition; (b) ICP etching forms a cylinder mesa feature; (c) silica sphere removal; (d) wet etching forms the microdisk with a mushroom-shaped structure.

structure was thoroughly cleaned with acetone, isopropanol, and deionized (DI) water. In Fig. 2(a), a dilute suspension of silica spheres in isopropanol was dispersed onto the sample surface using a spin-coating method at a low rotation speed (2000 rpm). ICP etching was then performed to get a cylindrical mesa feature [see Fig. 2(b)]. A smooth sidewall of the microdisks was achieved by using optimized ICP etching parameters. The chamber pressure was maintained at 10 mTorr, with the coil and platen power set to 500 W and 100 W, respectively. Cl_2, BCl_3, and He mixed gases were used with flow rates of 10 sccm, 10 sccm, and 5 sccm, respectively. The silica spheres were subsequently removed by water in an ultrasonic bath [see Fig. 2(c)]. Afterward, Si underneath the microdisk was etched by chemical etching to form a mushroom-shaped structure [see Fig. 2(d)]. Two different chemical etches, 20M diluted potassium hydroxide (KOH) solution and a 65% HF/HNO_3 (1:1) solution, were used to obtain the mushroom-shaped structure of microdisk lasers pivoted on Si. More importantly, this chemical etching can not only remove the damage generated in the ICP etching but also modify the microdisk sidewall, resulting in different sidewall roughness. Figures 3(a) and 3(d) show the top-view scanning electron microscope (SEM) images of the fabricated devices on Si etched by the KOH and HF/HNO_3 solutions, respectively. Figure 3(a) shows a microdisk of circular geometry with many irregular triangular prism-like shapes. In contrast, Fig. 3(d) shows a microdisk with smoother sidewalls. Figures 3(b) and 3(e) present 70°-tilted SEM images of the fabricated devices pivoted on Si etched by the KOH and HF/HNO_3 solutions, respectively. It is obvious that Si was etched laterally from the outer periphery to form a supporting pedestal. Figures 3(c) and 3(f) show the zoomed-in view of the sidewall in 70°-tilted SEM images of the disk etched by KOH and HF/HNO_3 solutions, respectively. Figure 3(c) shows the disk with rough sidewalls of stripe-patterns. This morphology is due to the etching-selectivity difference between the m-plane and the a-plane of GaN, which is typically observed in KOH etching of GaN.[34,35] Compared to the KOH solution, HF/HNO_3, with an almost zero etching rate of GaN, can be successfully used to achieve a smoother sidewall, as shown in Fig. 3(f).

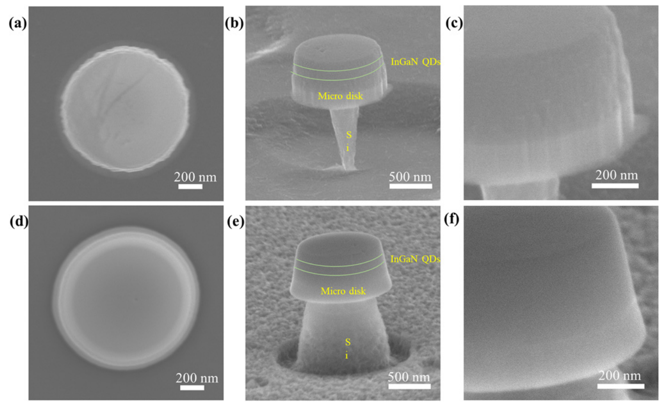

FIG. 3. (a) Top-view SEM image, (b) 70°-tilted SEM image, and (c) zoomed-in view of the sidewall in 70°-tilted SEM images of the disk etched by KOH. (d) Top-view SEM image, (e) 70°-tilted SEM image, and (f) zoomed-in view of the sidewall in the 70°-tilted SEM image of the disk etched by HF/HNO_3.

We probed the optical properties of the microdisk lasers using a micro-PL measurement system at room temperature. Figure 4(a) displays the measured PL spectra of the microdisk lasers etched by KOH at different excitation power densities. The sharp peaks in the spectra correspond to different WG modes. At low pumping power density, the QD microdisk exhibits a broad spontaneous emission spectrum with resonance peaks of the WG modes. The QD background spontaneous emission from the center of the microdisk does not couple to the cavity mode. As the pumping power density increases, the WG modes become stronger compared to the background spontaneous emission. The PL spectrum at a pump power intensity of 14.8 kW/cm^2 [see Fig. 4(b)] is well fitted with bi-Lorentzian curves, where the peak

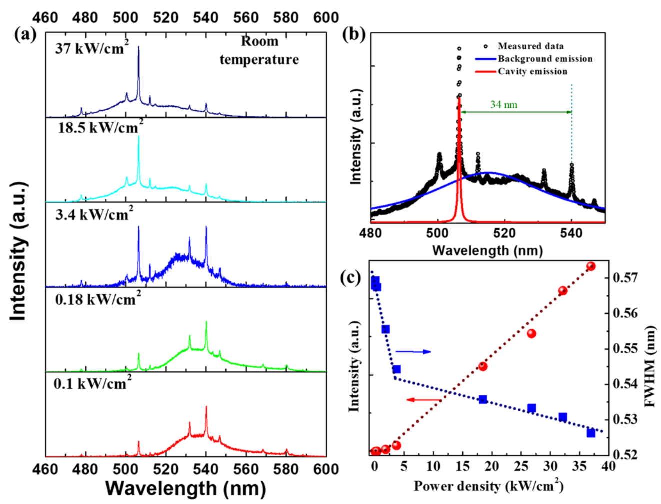

FIG. 4. (a) Emission spectra with the linear scale of the microdisk laser etched by KOH at various injection power densities at room temperature. (b) Emission spectra at a pumping excited power density of 14.8 kW/cm^2. (c) Collected intensity and FWHM of optical mode at 506 nm as a function of pumping power density.

intensity of both the broad InGaN QD PL background and narrow cavity modes are extracted. The free-spectral range (FSR) of the cavity modes can be calculated using $\Delta\lambda = \lambda^2/\pi N_{eff}$, where λ is the emission wavelength, R is the radius of the disk, and n_{eff} is the group effective index of refraction. The calculated FSR agrees well with the observed spacing of ~34 nm. The collected intensity (L–L curve) and FWHM for the emission peak at 506 nm as a function of excited power density are plotted in Fig. 4(c). The FWHM exhibits a dramatic reduction with increasing optical pumping power density, providing a signature of laser action. The cavity Q-factor was calculated accordingly to be $\lambda/\Delta\lambda = 955$. A clear threshold knee is observed in the L–L curve, and the threshold is extracted to be around 1.6 kW/cm^2. We attribute the low threshold of the microcavity lasers to the strong quantum confinement of carriers inside the QDs.

We have also found that the sidewall smoothness plays an important role in the thresholds of the microdisk lasers. Figure 5(a) shows the measured PL spectra of the microdisk lasers etched by HF/HNO_3 at different excitation power densities. At a low pumping power density of 15 W/cm^2, three resonance peaks for the WG modes were observed at 557 nm, 547 nm, and 522 nm. As the pumping power density increases to 76 W/cm^2, the intensity of optical mode at 522 nm emission is comparable with the optical mode at 547 nm. Furthermore, both these two modes are stronger than those of the optical mode at 557 nm. This type of mode competition can be avoided by increasing the stacked layers of QDs.[36,37] The mushroom-shaped geometry of the microdisk laser is not only advantageous for optically isolation but also insensitive to heating. Note that no peak wavelength shift of both devices etched by HF/HNO_3 and KOH can be observed with progressively increased pumping power, suggesting negligible thermal generation inside the disk region. As the pumping power density further increases to 1.5 kW/cm^2, the optical mode at 522 nm becomes dominant, with a FWHM of 0.2 nm. The cavity Q-factor was thereby calculated to be as high as 2610. Figure 5(b) shows a fitted curve of the measured spectra at a pump intensity of 18.5 kW/cm^2, including the broad InGaN QD PL background and the narrow cavity emission. Compared to the devices etched by KOH, these devices exhibit higher intensity of optical modes and lower background emission, indicating significant improvement of the optical confinement. It is believed that the difference in the lasing wavelength and Q-factor between the microdisk etched by KOH and HF/HNO_3 resulted from the different sidewall conditions. Our observation here confirms the previously reported influence of sidewall roughness on the WG mode resonance characteristics. The L–L curves of the optical mode at 522 nm as a function of pumping power density are shown in Fig. 5(c). A distinctive kink indicating the onset of lasing operation can be clearly seen. The threshold of the optical mode at 522 nm can be extracted to be as low as 76 W/cm^2. Compared to the microdisk lasers etched by KOH, the significantly improved threshold is attributed to the smoother sidewall conditions.[38] The electric fields are mainly localized at the edges of the microdisk in whispering gallery mode microdisk lasers. Scattering of light at the rough sidewall would induce optical losses. The sidewall roughness scatters some of the energy into the radiation continuum, inducing leakage of optical modes and thus increases threshold for lasing. It is worth noting that the thresholds of our microdisk lasers grown on Si are even lower than those directly grown on sapphire substrates lasing in the blue spectral region.[11]

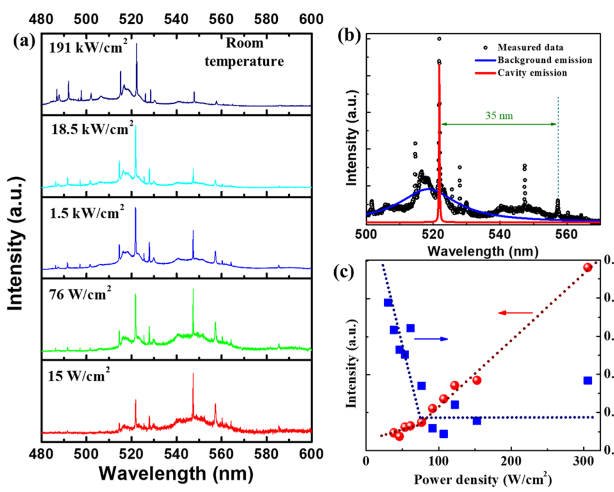

FIG. 5. (a) Emission spectra with the linear scale of the microdisk lasers etched by HF/HNO_3 at various injection power densities at room temperature. (b) Emission spectra at a pumping excited power density of 18.5 kW/cm^2. (c) Collected intensity and FWHM of optical mode at 522 nm as a function of pumping power density.

In conclusion, we have demonstrated room temperature CW lasing from green InGaN QD microdisk lasers directly grown on Si (111) substrates. Adopting QDs as the gain medium and improving the sidewall smoothness, we achieved an ultra-low threshold of 76 W/cm^2 and a high Q-factor of 2610. Our results here suggest a promising path toward integrating compact and energy-efficient green light sources onto mainstream Si platforms.

This work was supported in part by grants (Nos. 16216017, T23-407/13N-2, 16302717, and C6013-16E) from the Research Grants Council of Hong Kong. The authors thank the MCPF and NFF of HKUST for technical support. Helpful discussions with Professor Evelyn Hu and Dr. Yu Han are also acknowledged.

DATA AVAILABILITY

The data that support the findings of this study are available within the article.

REFERENCES

[1] S. Pimputkar, J. S. Speck, S. P. DenBaars, and S. Nakamura, Nat. Photonics **3**, 179 (2009).
[2] S. Nakamura, Science **281**, 956 (1998).
[3] H. Jiang, R. Zhu, Q. Lyu, and K. M. Lau, IEEE Electron Device Lett. **40**, 530 (2019).
[4] Y. Wu, X. Sun, Z. Shi, Y. Jia, K. Jiang, J. Ben, C. Kai, Y. Wang, W. Lü, and D. Li, Nanoscale Adv. **2**, 1854 (2020).
[5] Y. Zhao, S. Tanaka, C.-C. Pan, K. Fujito, D. Feezell, J. S. Speck, S. P. DenBaars, and S. Nakamura, Appl. Phys. Express **4**, 082104 (2011).
[6] Y. Sun, K. Zhou, Q. Sun, J. P. Liu, M. X. Feng, Z. C. Li, Y. Zhou, L. Q. Zhang, D. Y. Li, S. M. Zhang, M. Ikeda, S. Liu, and H. Yang, Nat. Photonics **10**, 595 (2016).
[7] H. Ohta, S. P. DenBaars, and S. Nakamura, J. Opt. Soc. Am. B **27**, B45 (2010).
[8] S. Essaian and J. Khaydarov, Opt. Rev. **19**, 400 (2012).
[9] J. J. Wierer, Jr., J. Y. Tsao, and D. S. Sizov, Phys. Status Solidi C **11**, 674 (2014).
[10] C. Zhao, C. W. Tang, B. Lai, G. Cheng, J. Wang, and K. M. Lau, Photonics Res. **8**, 750 (2020).

[11]A. C. Tamboli, E. D. Haberer, R. Sharma, K. H. Lee, S. Nakamura, and E. L. Hu, Nat. Photonics **1**, 61 (2007).
[12]K. J. Vahala, Nature **424**, 839 (2003).
[13]S. L. McCall, A. F. J. Levi, R. E. Slusher, S. J. Pearton, and R. A. Logan, Appl. Phys. Lett. **60**, 289 (1992).
[14]U. Mohideen, R. E. Slusher, F. Jahnke, and S. W. Koch, Phys. Rev. Lett. **73**, 1785 (1994).
[15]H. W. Choi, K. N. Hui, P. T. Lai, P. Chen, X. H. Zhang, S. Tripathy, J. H. Teng, and S. J. Chua, Appl. Phys. Lett. **89**, 211101 (2006).
[16]K. H. Li, W. Y. Fu, Y. F. Cheung, K. K. Y. Wong, Y. Wang, K. M. Lau, and H. W. Choi, Optica **5**, 564 (2018).
[17]M. Feng, J. Wang, R. Zhou, Q. Sun, H. Gao, Y. Zhou, J. Liu, Y. Huang, S. Zhang, M. Ikeda, H. Wang, Y. Zhang, Y. Wang, and H. Yang, IEEE J. Sel. Top. Quantum Electron. **24**, 1 (2018).
[18]J. Sellés, V. Crepel, I. Roland, M. El Kurdi, X. Checoury, P. Boucaud, M. Mexis, M. Leroux, B. Damilano, S. Rennesson, F. Semond, B. Gayral, C. Brimont, and T. Guillet, Appl. Phys. Lett. **109**, 231101 (2016).
[19]X. Zhang, Y. F. Cheung, Y. Zhang, and H. W. Choi, Opt. Lett. **39**, 5614 (2014).
[20]M. Athanasiou, R. Smith, B. Liu, and T. Wang, Sci. Rep. **4**, 7250 (2014).
[21]J. Wang, M. Feng, R. Zhou, Q. Sun, J. Liu, X. Sun, X. Zheng, M. Ikeda, X. Sheng, and H. Yang, Opt. Express **28**, 12201 (2020).
[22]Y. Zhang, X. Zhang, K. H. Li, Y. F. Cheung, C. Feng, and H. W. Choi, Phys. Status Solidi A **212**, 960 (2015).
[23]M. Zhang, A. Banerjee, C.-S. Lee, J. M. Hinckley, and P. Bhattacharya, Appl. Phys. Lett. **98**, 221104 (2011).
[24]D. Bimberg, N. Kirstaedter, N. N. Ledentsov, Z. I. Alferov, P. S. Kop'ev, and V. M. Ustinov, IEEE J. Sel. Top. Quantum Electron. **3**, 196 (1997).
[25]D. Wang, T. Zhu, R. A. Oliver, and E. L. Hu, Opt. Lett. **43**, 799 (2018).
[26]M. Bürger, G. Callsen, T. Kure, A. Hoffmann, A. Pawlis, D. Reuter, and D. J. As, Appl. Phys. Lett. **103**, 021107 (2013).
[27]I. Aharonovich, A. Woolf, K. J. Russell, T. Zhu, N. Niu, M. J. Kappers, R. A. Oliver, and E. L. Hu, Appl. Phys. Lett. **103**, 021112 (2013).
[28]Q. Xie, A. Madhukar, P. Chen, and N. P. Kobayashi, Phys. Rev. Lett. **75**, 2542 (1995).
[29]N. N. Ledentsov, V. A. Shchukin, M. Grundmann, N. Kirstaedter, J. Böhrer, O. Schmidt, D. Bimberg, V. M. Ustinov, A. Yu Egorov, A. E. Zhukov, P. S. Kop'ev, S. V. Zaitsev, N. Yu Gordeev, Z. I. Alferov, A. I. Borovkov, A. O. Kosogov, S. S. Ruvimov, P. Werner, U. Gösele, and J. Heydenreich, Phys. Rev. B **54**, 8743 (1996).
[30]C. Adelmann, J. Simon, G. Feuillet, N. T. Pelekanos, B. Daudin, and G. Fishman, Appl. Phys. Lett. **76**, 1570 (2000).
[31]J. Zhang, M. Hao, P. Li, and S. J. Chua, Appl. Phys. Lett. **80**, 485 (2002).
[32]K. Tachibana, T. Someya, and Y. Arakawa, Appl. Phys. Lett. **74**, 383 (1999).
[33]Y. D. Jho, J. S. Yahng, E. Oh, and D. S. Kim, Phys. Rev. B **66**, 035334 (2002).
[34]R. Debnath, J. Y. Ha, B. Wen, D. Paramanik, A. Motayed, M. R. King, and A. V. Davydov, J. Vac. Sci. Technol., B **32**, 021204 (2014).
[35]Y. Jung, K. H. Baik, M. A. Mastro, J. K. Hite, C. R. Eddy, and J. Kim, Phys. Chem. Chem. Phys. **16**, 15780 (2014).
[36]T. Zhou, M. Tang, G. Xiang, X. Fang, X. Liu, B. Xiang, S. Hark, M. Martin, M.-L. Touraton, T. Baron, Y. Lu, S. Chen, H. Liu, and Z. Zhang, Optica **6**, 430 (2019).
[37]A. E. Zhukov, A. R. Kovsh, N. A. Maleev, S. S. Mikhrin, V. M. Ustinov, A. F. Tsatsul'nikov, M. V. Maximov, B. V. Volovik, D. A. Bedarev, Y. M. Shernyakov, P. S. Kop'ev, Z. I. Alferov, N. N. Ledentsov, and D. Bimberg, Appl. Phys. Lett. **75**, 1926 (1999).
[38]B. E. Little and S. T. Chu, Opt. Lett. **21**, 1390 (1996).